Crystallization of Poly(ethylene-co-octene): Melt Memory Effects on First Order Kinetics

A. Häfele, B. Heck, T. Hippler, T. Kawai, P. Kohn and G. Strobl

Physikalisches Institut, Albert-Ludwigs-Universität Freiburg

79104 Freiburg, Germany

Abstract

Dilatometric and X-ray scattering experiments of the crystallization kinetics of a sample of poly(ethylene-co-octene) show pronounced melt memory effects, i.e., the shapes of isotherms and characteristic times vary systematically with the temperature of the melt prior to cooling to the crystallization temperature. The temperature range of the effect is limited; crystallization kinetics remains constant below a melt temperature $T_{\mathrm{m}}^{\mathrm{l}}$ and above a melt temperature $T_{\mathrm{m}}^{\mathrm{h}}$ and varies only in-between. Analysis shows that the melt memory effect is caused by a variation of the characteristic time of a first order crystallization process. The process can be assigned to the in-filling of crystallites into objects of a previously generated precursor structure.

1 Introduction

As described and discussed in the foregoing paper, polyethylene with a moderate content of statistically distributed octene-units ('PEcO14') shows peculiarities in the crystallization behavior. After cooling a melt to a preset crystallization temperature, at first a precursor structure appears. Observations in a polarizing optical microscope show throughout the viewing field a diffuse structure with variations in the μm-range. These objects are subsequently filled in statistical manner with small crystallites whose orientations are correlated so that the birefringence of the objects continuously increases. Fig.1 gives an example of this in-filling process as it shows up in in-situ studies with an atomic force microscope. Simultaneous with this peculiar crystallization mode, spherulites are nucleated and grow. The growth ends at a certain size which is common to all spherulites. Fig.2 presents an example of the final structure reached after an isothermal crystallization at 93 °C. One notes that the spherulites fill the sample volume only partially but the precursor objects are found everywhere, outside of the spherulites and also as inclusions. Time dependent measurements of the crystallization kinetics by dilatometry or X-ray scattering indicate an increase of the crystallinity before saturation according to a power law $\phi_c \sim t^\nu$ with an exponent $\nu \simeq 1.5$. Such a law speaks in favour of a dominance of the in-filling process over the spherulite growth since the latter would lead to $\nu = 3$.

Polymer crystallization from a melt is often accompanied by memory effects. If a semicrystalline polymer is melted and then crystallized again, the time required for the second crystallization often varies with the temperature of the melt and the period of annealing in the molten stage. Discussions of this effect usually are based on an assumed persistence of nuclei [1][2][3][4][5]. This is a reasonable explanation as long as the shape of the isotherms is constant and variations concern only the characteristic time. There are also cases where a change in the power law exponent is observed and they need other explanations [6]. Our sample under study, PEcO14, exhibits also pronounced, characteristic melt memory effects. We found it worthwhile

to study them in greater detail and thereby obtained further insights in the mechanism of crystallization. The experimental results - again obtained using dilatometry, simultaneous small angle and wide angle X-ray scattering, polarizing optical microscopy, light scattering, and atomic force microscopy - led us to the conclusion that

- the creation of the crystals which continuously fill the objects of the precursor structure follows a first order kinetics,
- the melt memory effects originate from changes in the creation rate.

2 Experimental

The sample under study was the same as used previously, a metallocene catalyzed poly(ethylene-co-octene) with 14% per weight of co-units supplied by Dow Chemicals Europe. It had a molar mass $M_{\mathrm{n}} = 30200$ and a polydispersity index $M_{\mathrm{w}}/M_{\mathrm{n}} = 3.0$.

As we used here the same experimental equipment as in the first part of the work

- a dilatometer,
- a camera for simultaneous small angle (SAXS) and wide angle (WAXS) X-ray scattering experiments,
- a polarizing optical microscope,
- a light scattering device, and
- an atomic force microscope

we refer for the description of the different tools and the associated evaluation methods to the first paper [7].

3 Results

Fig.3 presents a series of dilatometer curves $v(t)$ (v: specific volume) measured for crystallizations at a fixed crystallization temperature, T_c=93 °C, and various temperatures of the melt, T_m, prior to cooling. To have a reliable comparison we followed in all measurements the same temperature protocol, namely:

1. 10 minutes of annealing in the melt at 160 °C
2. rapid cooling to 93 °C and complete crystallization
3. heating to a melt temperature T_m and annealing for 20 minutes
4. rapid cooling to the crystallization temperature T_c and starting the experiment when this temperature is reached.

The dilatometric curves include at the beginnings the final decrease to the crystallization temperature, then show a plateau from where the crystallization induced decay then starts. The effect of the melt temperature on the crystallization kinetics is obvious. Interestingly, one finds changes only in a limited temperature range, that between 120 °C and 127 °C. On both sides no further variations are observed, neither for lower, nor for higher melt temperatures.

Fig.4 shows the two dilatometric curves registered in the limits of low ($T_m < T_m^l = 120$ °C) and high melt temperatures ($T_m > T_m^h = 127$ °C) for various crystallization temperatures T_c. The memory effect exists for all chosen T_cs.

There is a remarkable feature in the curves of Fig.3: Independent of the chosen melt temperature they finally all end up at the low T_m limiting curve. According to Fig.4 this is valid for all crystallization temperatures - the limiting curves for high melt temperatures coalesce in the long time limit with the respective low T_m limiting curve. The observations indicate straightforwardly that final crystallinities are independent of the chosen melt temperature.

Figs.5 and 6 present the crystallization isotherms

$$\Delta v(t) = v(0) - v(t)$$

7 derived from the dilatometer curves in log-log plots ($v(0)$ is the initial value of the specific volume reached after the rapid cooling before the onset of crystallization). The initial slope of the low T_m limiting isotherms indicates a power law exponent of $\nu = 1$, that of the high T_m limiting curves of $\nu = 1.5$. In correspondence to the dilatometric curves all the crystallization isotherms finally coincide with the respective low T_m limiting curve.

Figs.7 and 8 show the results of an equivalent series of experiments carried out by simultaneous small angle and wide angle X-ray scattering. The first of the two figures presents crystallization isotherms in terms of the Porod coefficient $P(t)$ (see ref.[7] for the definition of P) obtained at $T_\mathrm{c} = 90$ °C for various T_ms; again two limiting curves are found. The second figure gives the two limiting curves for various T_cs. In Fig.8 both, the time dependence of the Porod coefficient, $P(t)$, and of the intensity of the 110-Bragg reflection, $I_\mathrm{B}(t)$ are shown for all the curves. Obviously both agree with each other. Hence, the development of the Porod coefficient is associated with the formation of crystalline lamellae exclusively. We determined also the crystal thickness d_c for various T_ms and could not find any effect of the melt temperature, for example, d_c is constantly at 5.0nm for $T_\mathrm{c} = 90$ °C.

Fig.9 compares the isotherms measured in the dilatometer with corresponding ones obtained by SWAXS. The comparison is carried out for the two limiting curves, registered at 91 °C and 92 °C respectively. The temperature differencies were accounted for by shifts along the $\log t$-axis. One notes a perfect agreement. Hence, the densification registered in the dilatometer is due to the crystal formation only. If the formation of the precursor structure should also be accompanied by a densification, which is probable, it is too low to be detected by small angle X-ray scattering or dilatometry.

Different melt temperatures prior to the cooling to T_c result in clear changes in the morphology in the μm-range as observed in the POM under crossed nicols. Fig.10 collects some images of final structures resulting at T_c =93 °C for different T_ms. A decrease in the temperature of the melt in the sensitive range leads to a general decrease in the brightness. In addition, at the lower T_ms spherulites can no longer be observed. The findings indicate a decrease in the object sizes, both, for the objects of the precursor structure and, much stronger, for the spherulites. This can be checked by depolarized light scattering experiments. Fig.11 shows scattering intensity distributions, $I^{hv}(q)$ ($q = 4\pi \sin\theta/\lambda$), as measured for the azimuthal average and along the equator. The two figures refer to different temperatures of the melt. The precursor objects show up in the equatorial scattering and the spherulites give an additional contribution with a maximum at $q = 4.09/R$ ($R:$ spherulite radius) and a vanishing intensity in forward direction ($q = 0$). As can be seen, the decrease in the melt temperature results in an increase of the half-width of the precursor component from 0.4 to 1μm^{-1} and an increase of the peak position of the spherulite structure factor from 0.25 to 1.4μm^{-1}. Hence, we have indeed a decrease in size for both objects and it is much larger for the spherulites.

The decrease in the brightness of the POM images can also be registered in a quantitative way. An appropriate measure is obtained by a summation over the intensity values stored in all pixels of the CCD-chip. Fig.12 presents corresponding results. In conformance with the images there is no change in the final brightness when the melt temperature is varied between 160 °C and 122 °C, but then a decrease sets in. An at first unexpected result came up when we compared the time dependence of this brightness parameter with dilatometric isotherms. Fig.13 shows such a comparison for the two limiting curves: The curves essentially agree, their shapes are quite similar. One has to conclude that the value of the brightness parameter is proportional to the number of the birefringent crystallites; each one contributes in equal manner to the total degree of depolarization. The same result would have been obtained when carrying out a depolarized

scattering experiment, rather than counting the numbers of photons with changed polarization in the image. In fact, such measurements have already been carried out long ago and addressed as a determination of the 'depolarization factor' which is indeed proportional to the number of birefringent objects [8].

4 Discussion

Even if the spherulites show up clearly in the POM images it is the statistical in-filling of crystallites which dominates the kinetics of crystallization in the system. The observed power law with exponents near to one demonstrates this quite clearly. Correspondingly, the memory effects are mainly due to a variation of the rate of crystal nucleations within the objects of the precursor structure. According to the dilatometrically determined isotherms crystallization kinetics differs for different T_{m}s during the first stages, but becomes equal later-on. Such a behavior can be generally described by a time dependent crystallinity, $\phi_{\mathrm{c}}(t)$, of the form

$$\phi_{\mathrm{c}}(t) = \phi_{\mathrm{c}}(\infty) f_1(t) f_2(t) \tag{1}$$

with

$$f_1(t=0) = f_2(t=0) = 0$$

and normalizations

$$f_1(t \to \infty) = f_2(t \to \infty) = 1 \quad .$$

Here, $f_1(t)$ is a slowly varying function to be identified with the low T_{m} limiting isotherm at the chosen crystallization temperature. With increasing T_{c} it shifts to longer times as shown by the curves plotted with filled symbols in Fig.6. The second function, $f_2(t)$, describes the effect of the melt temperature for a fixed T_{c} and varies with T_{m}. Employing Eq.(1), $f_2(t)$ can be determined by a calculation of the ratio between an isotherm $\Delta v(t)$ measured for some $T_{\mathrm{m}}, T_{\mathrm{c}}$ and the low T_{m} limiting isotherm $\Delta v(t; T_{\mathrm{m}}^{\mathrm{l}})$ at the same T_{c}. Results of such calculations

are presented in Fig.14 for various crystallizations at T_c =93 °C and in Fig.15 for the high T_m limiting curves at all T_cs. The results are enlightening: All the functions $f_2(t)$ have the shape of a first order kinetical process; as shown in the figure, their slope in a log-log representation is equal to one. The assignment of this process is obvious: It can be associated with the in-filling of the crystallites. This takes place with a characteristic time given by the crystal nucleation rate within the precursor object. The experiments tell us that this rate can be affected by the temperature of the melt and the changes produce the memory effect, In addition, the rate depends as expected on T_c. Reflecting a first order kinetical process , the curves $f_2(t)$ have all a similar shape, being only shifted along the $\log t$-axis with T_c and T_m.

What is the meaning of the function $f_1(t)$? We think, that the answer can be given by a scheme as it is shown in Fig.16. The spherical objects are meant to be representatives of the volume occupied by the objects of the precursor phase which grows slowly in time. In the limit of low melt temperatures, T_m^l, they are always filled with a maximum density of crystallites. This is the situation shown in the upper row. For higher melt temperatures and the associated lower nucleation rates, the filling process is delayed. The function $f_1(t)$ in Eq.(1) thus describes the growth of the volume occupied by the objects of the precursor phase. The experimental low T_m limiting curves show at the beginning a regime where the crystallinity increases proportional to the time, i.e., they also start with an in-filling process. This part of the isotherm is not included in the scheme; it begins with already completely filled objects.

Reviewing all quantitatively evaluated experiments, i.e., dilatometry, SWAXS and the brightness measurements, one must resume that they all detect crystals only, under all experimental conditions, i.e., for all T_cs and T_ms. There are no signals from the objects of the precursor structure, although their existence seems to be ensured considering

- their function as a container which offers a crystal nucleation rate much higher than that of the free melt,

- the generation of an orientational texture of the crystallites within one object.

A mesomorphic phase with liquid crystal-like properties could provide such a surrounding. That it cannot be observed in measurements sensitive to density changes would not be astonishing considering that the density difference between the isotropic and the nematic state of a low molar mass liquid crystal is only in the order of 10^{-3}g cm^{-3}. A direct characterization needs other experiments; the techniques applied here are insufficient to reach this aim.

Acknowledgements

Support of this work by the Deutsche Forschungsgemeinschaft is gratefully acknowledged. Thanks are also due to the 'Fonds der Chemischen Industrie' for financial help.

References

[1] B. Wunderlich. *Macromolecular Physics - Vol.2*, page 52. Academic Press, 1976.

[2] B. Fillon, J.C. Wittmann, B. Lotz, and A. Thierry. *J.Polym.Sci.,Polym.Phys.*, 31:1383, 1993.

[3] Y.P. Kannah, W.P. Kuhn, J.E. Macur, A.F. Messa, N.S. Murthy, A.C. Reimschuessel, R.L. Schneider, J.P. Sibilia, A.J. Signorelli, and T.J. Taylor. *J.Polym.Sci.,Polym.Phys.*, 33:1023, 1995.

[4] G.C. Alfonso and A. Ziabicki. *Colloid Polym. Sci.*, 273:317, 1995.

[5] P. Supaphol and J. Lin. *Polymer*, 42:9617, 2001.

[6] B. Heck and G. Strobl. *Colloid Polym Sci*, 282:5117, 2004.

[7] A. Häfele, B. Heck, T. Hippler, T. Kawai, P. Kohn, and G. Strobl. *Eur.Phys.J.-E*, submitted, 2004.

[8] A. Schram. *Kolloid Z.u.Z.Polym.*, 151:18, 1957.

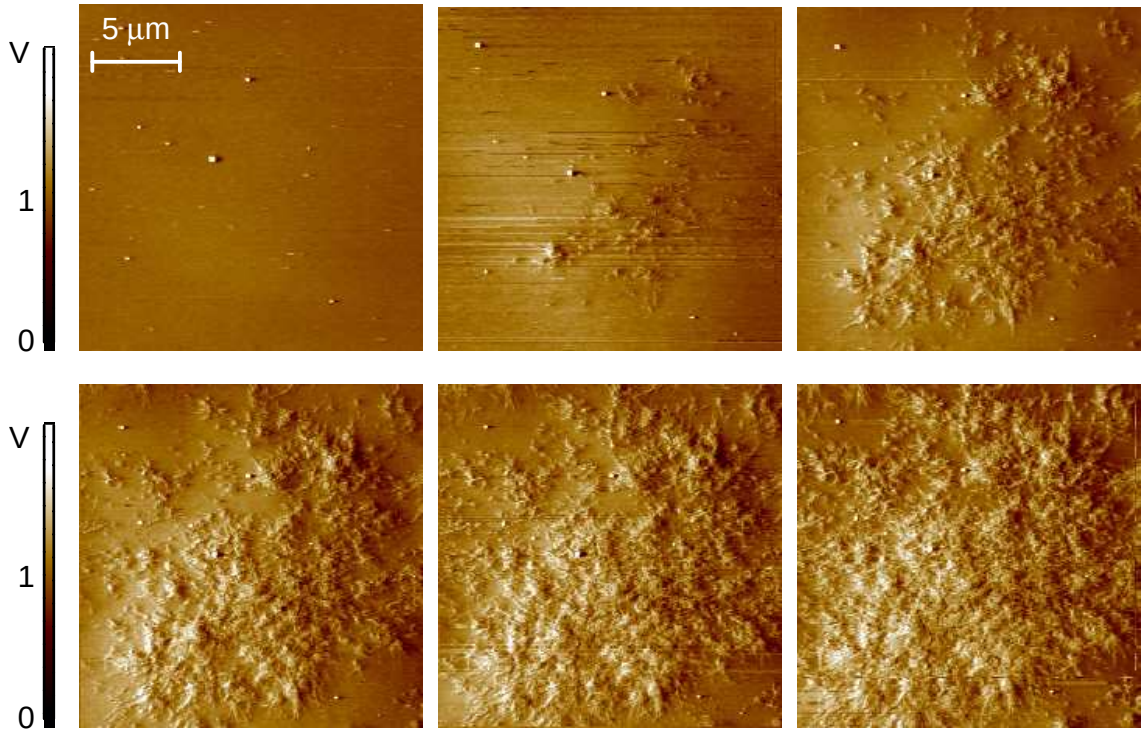

Figure 1: PEcO14: AFM tapping mode images (phase contrast) obtained during an isothermal crystallization at 92 °C

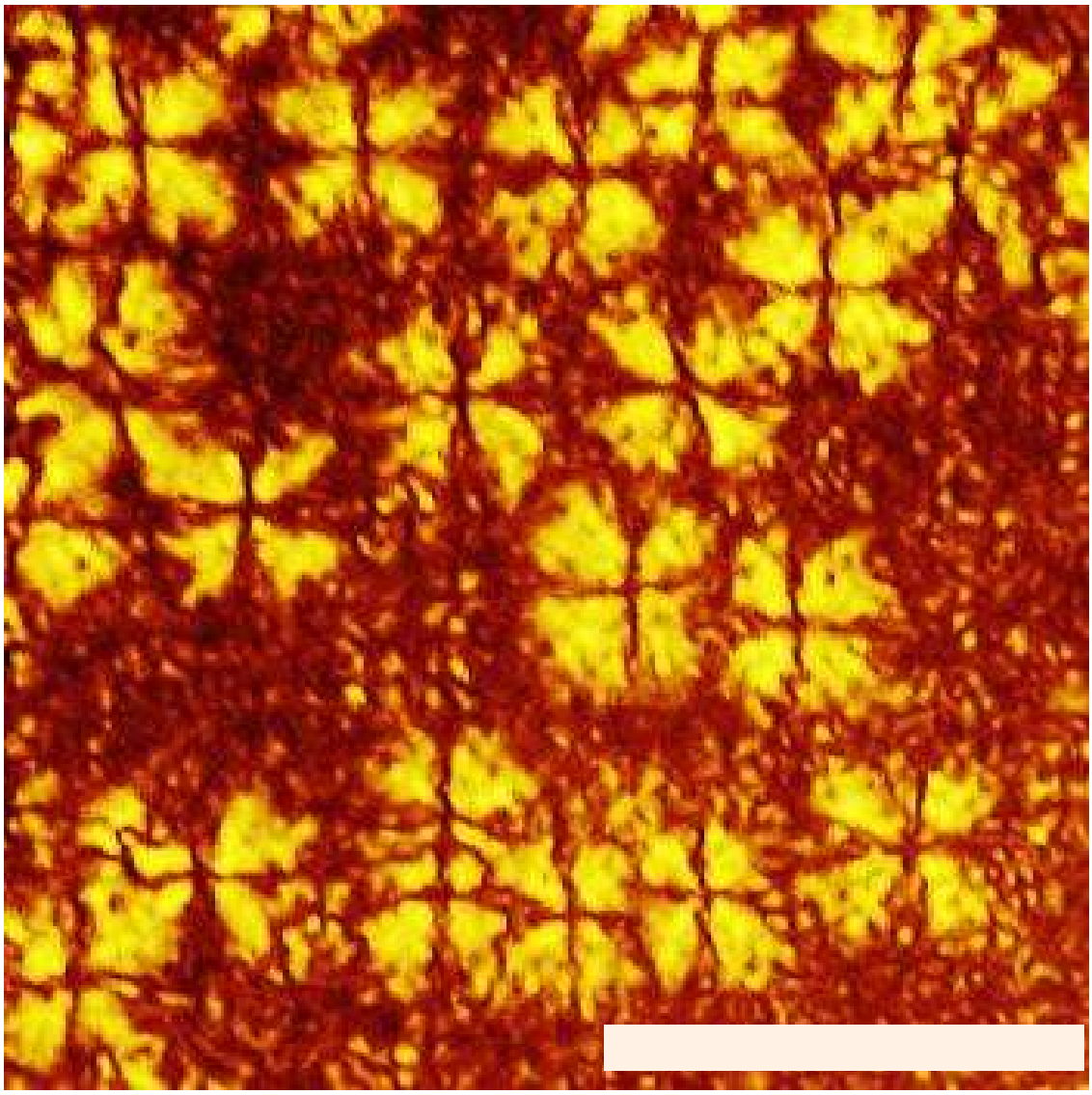

Figure 2: PEcO14: POM image of the final state reached after an isothermal crystallization at 93 °C. The prior melt temperature was 160 °C. The stick length is 100μm.

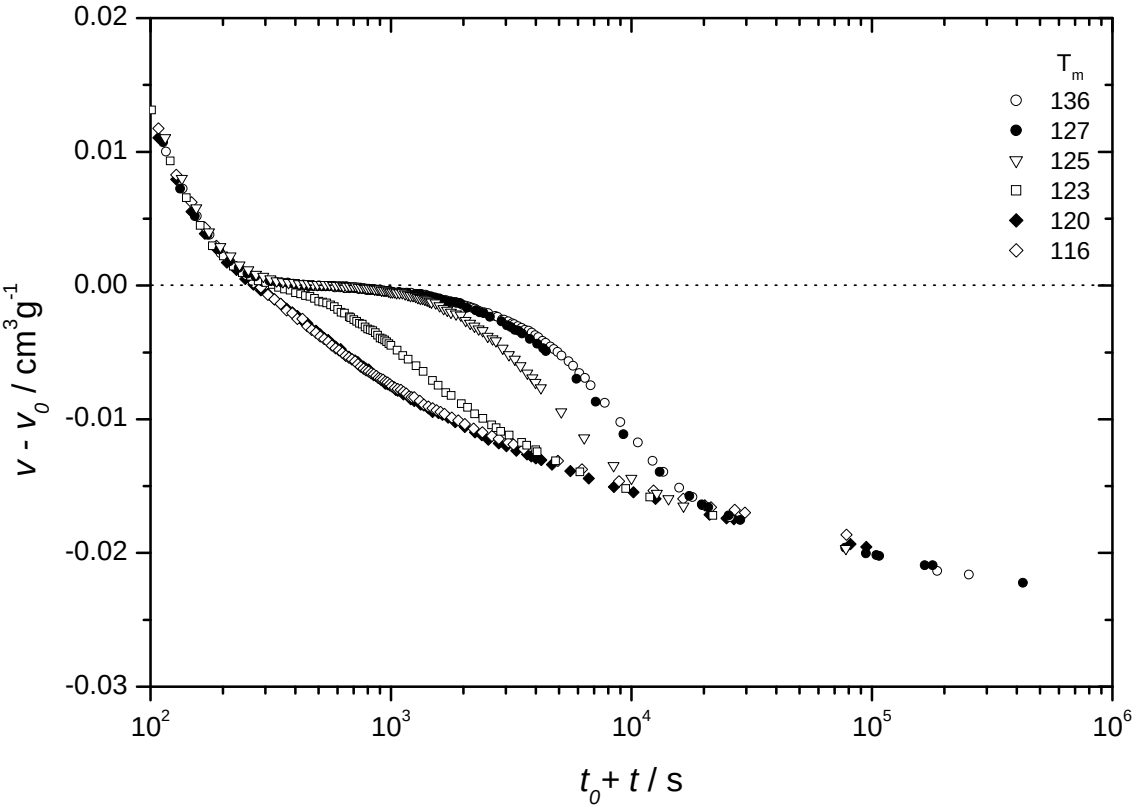

Figure 3: Time dependent volume changes observed in a dilatometer after cooling a melt to T_c = 93 °C. The melt temperatures prior to cooling varied between T_m = 116 °C and 136 °C

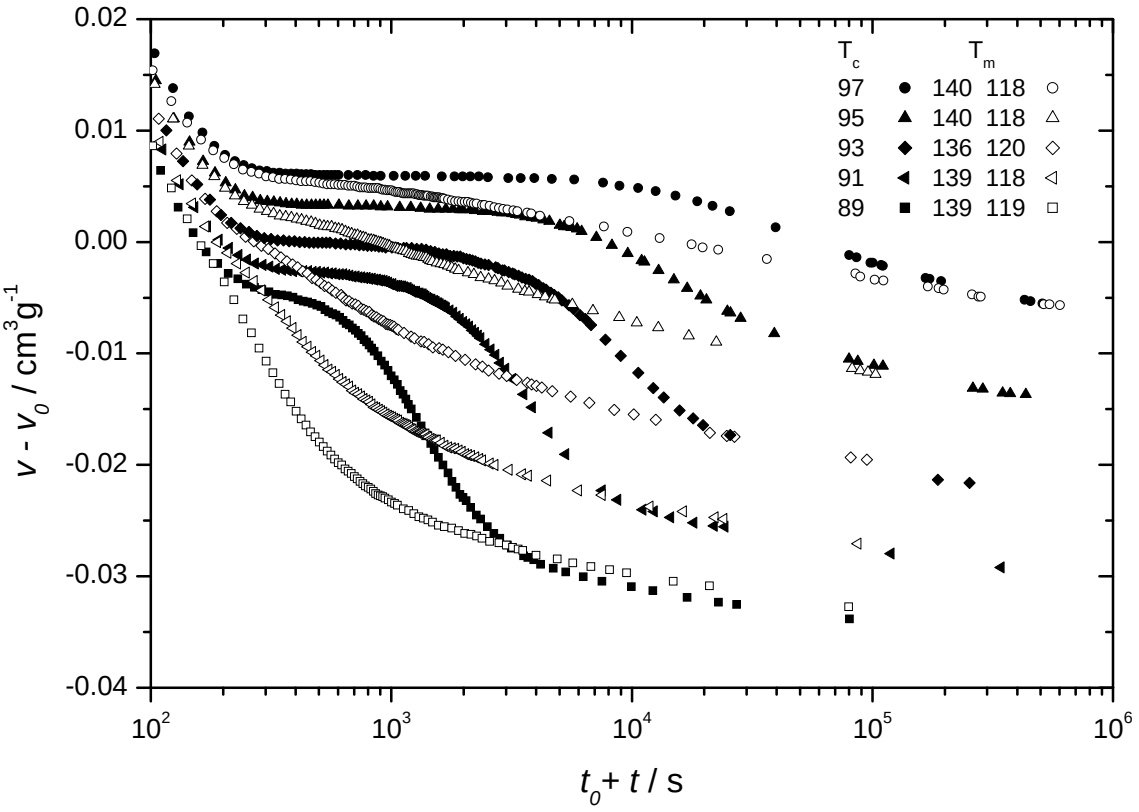

Figure 4: Time dependent volume changes observed in a dilatometer at the indicated crystallization temperatures T_c after cooling the melt. Prior to cooling the melt was kept either at 118-120 °C (*open symbols*) or at 136-140 °C (*filled symbols*)

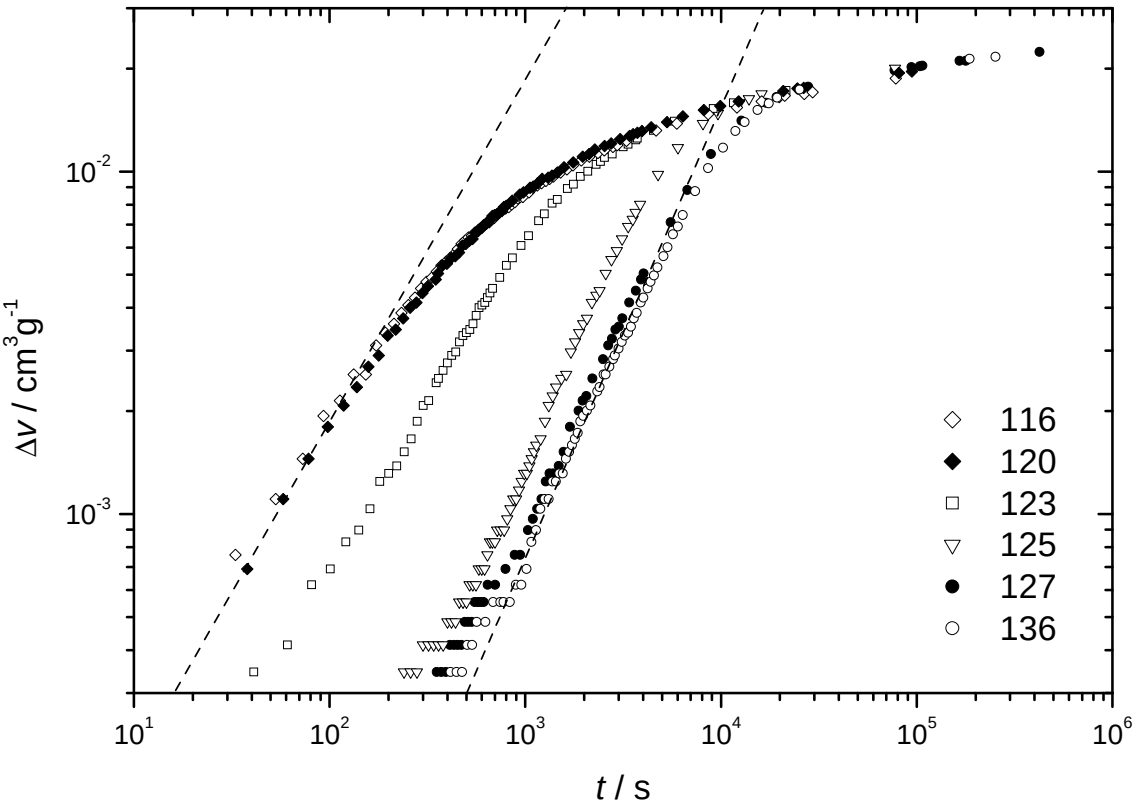

Figure 5: Dilatometric crystallization isotherms $\Delta v(t)$ for $T_\mathrm{c} = 93$ °C and various melt temperatures T_m as derived from Fig.3

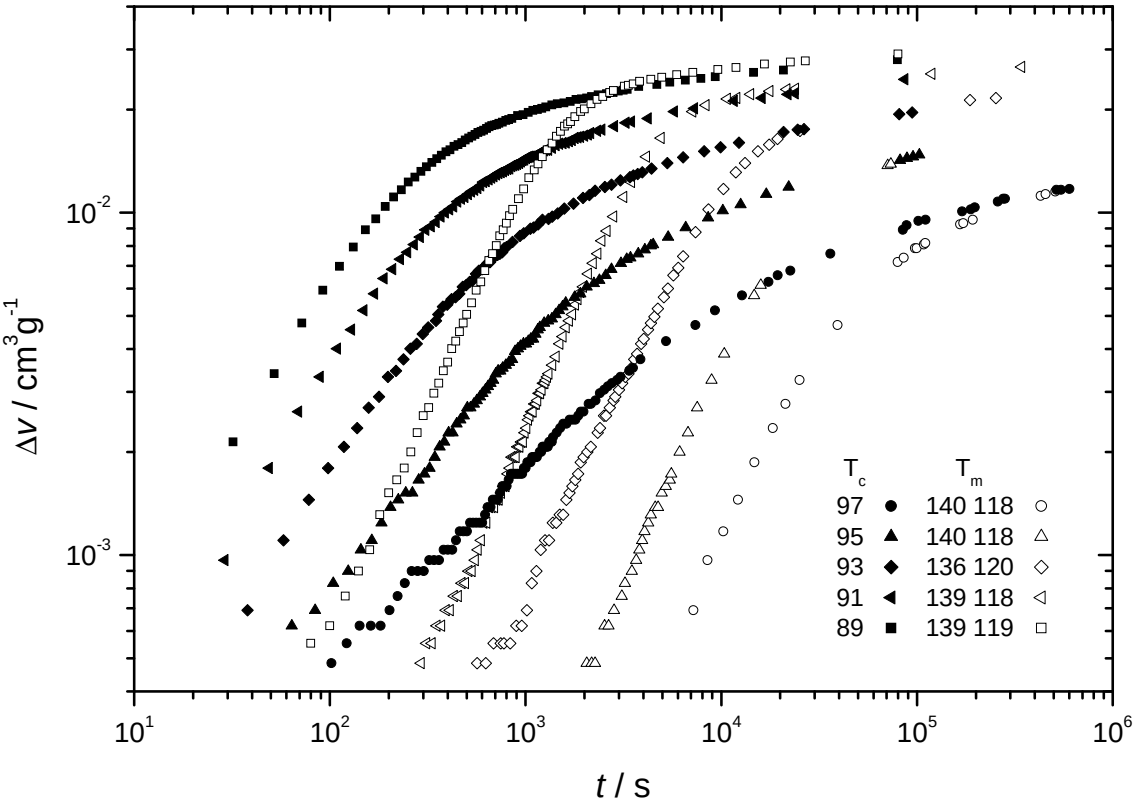

Figure 6: Derived from the curves in Fig.4: Dilatometric crystallization isotherms for various T_cs in the limit of a high or a low temperature melt respectively (T_m above 127 °C or below 120 °C)

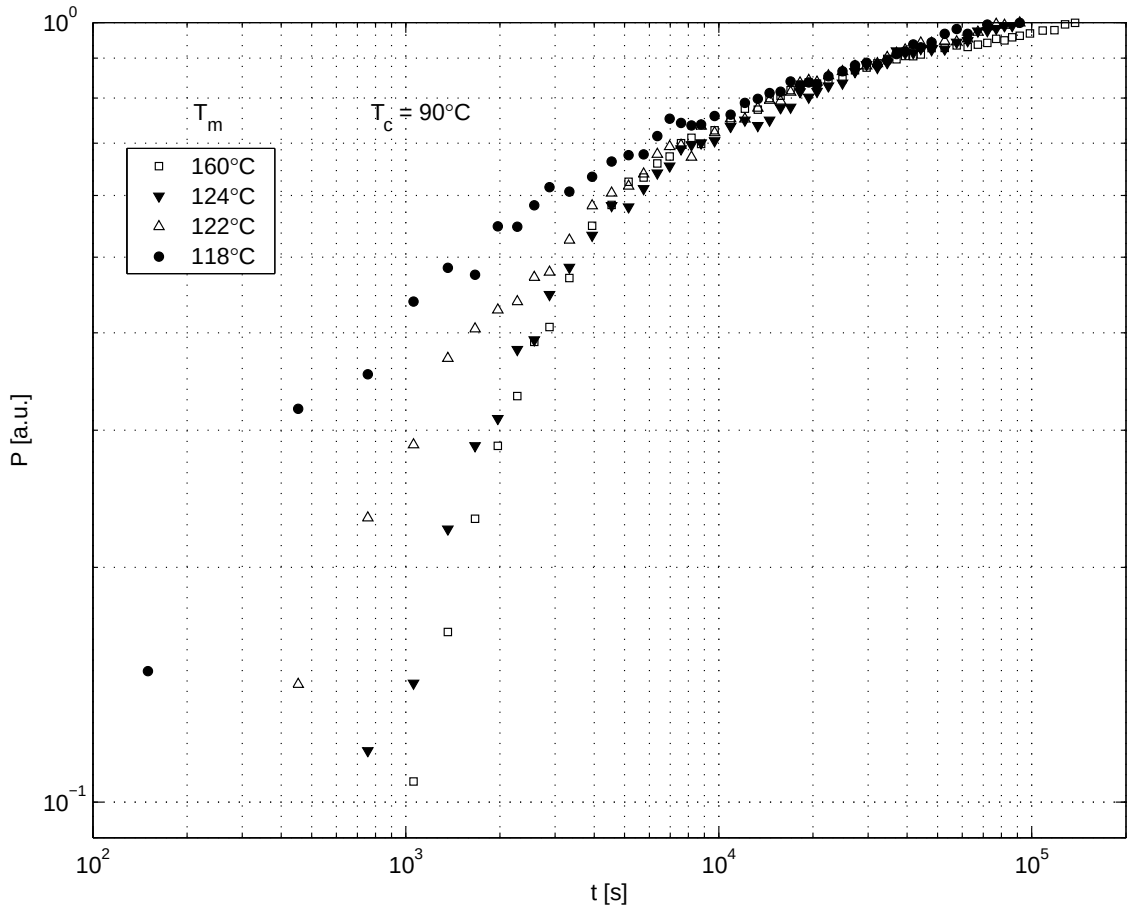

Figure 7: PEcO14: Development with time of the Porod coefficient P during isothermal crystallizations at 90 °C choosing various melt temperatures T_{m}

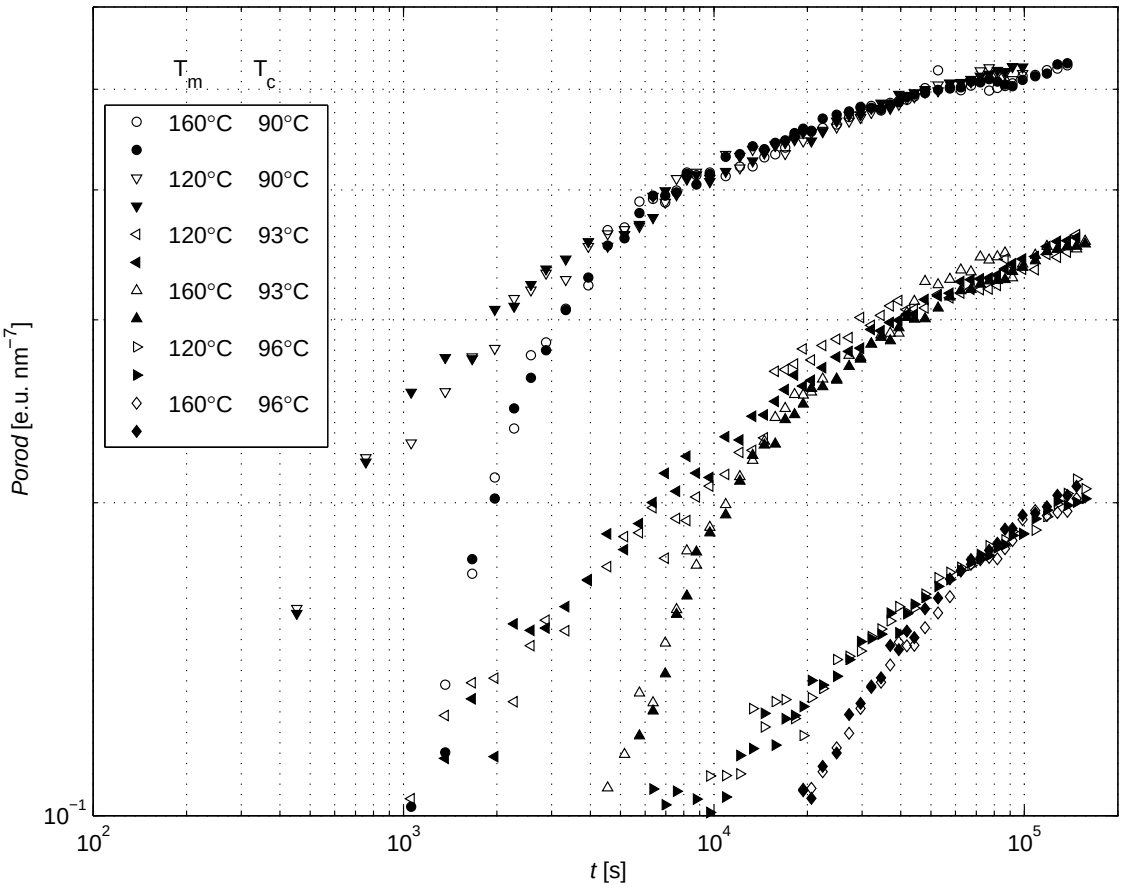

Figure 8: Development with time of the Porod coefficient P (*open symbols*) and the intensity I_{B} of a Bragg reflection (*filled symbols*) during isothermal crystallizations ($T_{\mathrm{c}} = 90$ °C, 93 °C and 96 °C) for two different melt temperatures prior to cooling ($T_{\mathrm{m}} = 120$ °C and 160 °C)

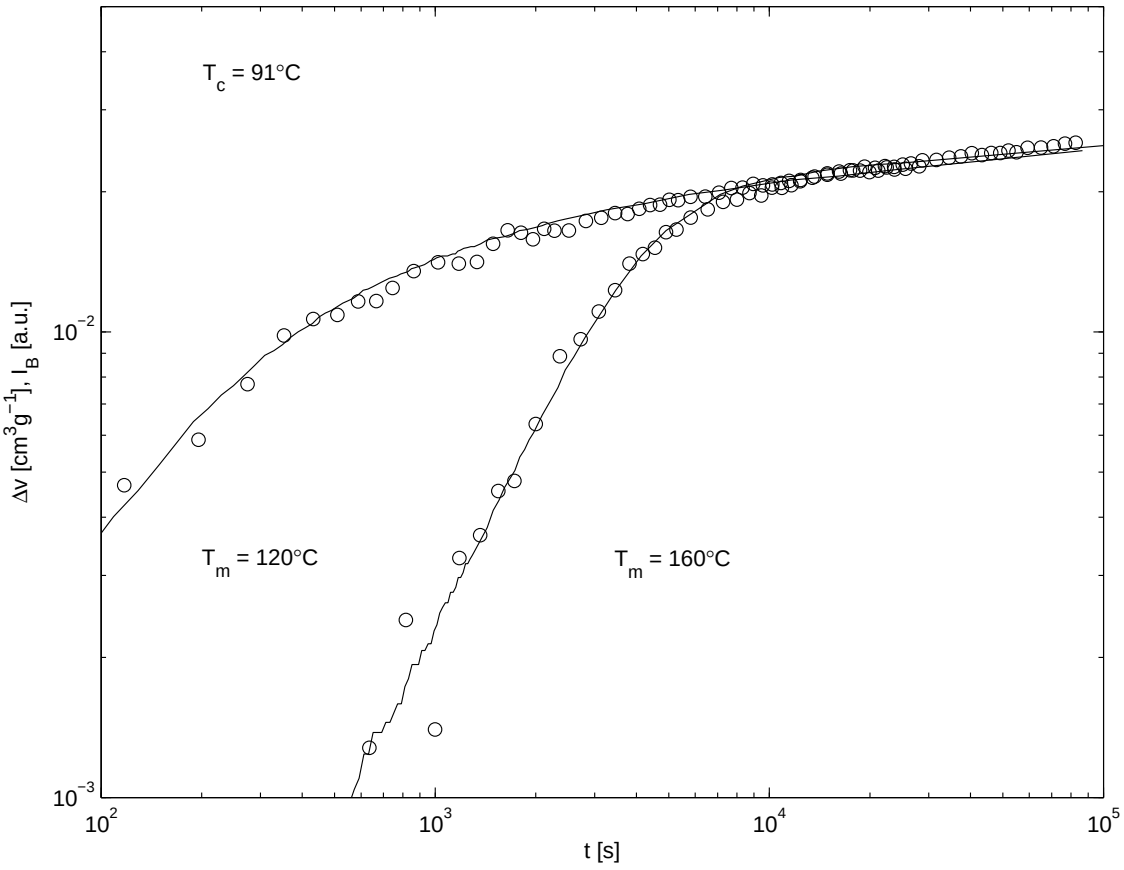

Figure 9: Isothermal crystallizations ($T_{\mathrm{c}} = 91$ °C) for two different melt temperatures prior to cooling ($T_{\mathrm{m}} = 120$ °C and 160 °C). Comparison of the isotherms $\Delta v(t)$ and $I_{\mathrm{B}}(t)$ obtained by dilatometry (*line*) and WAXS (*open symbols*)

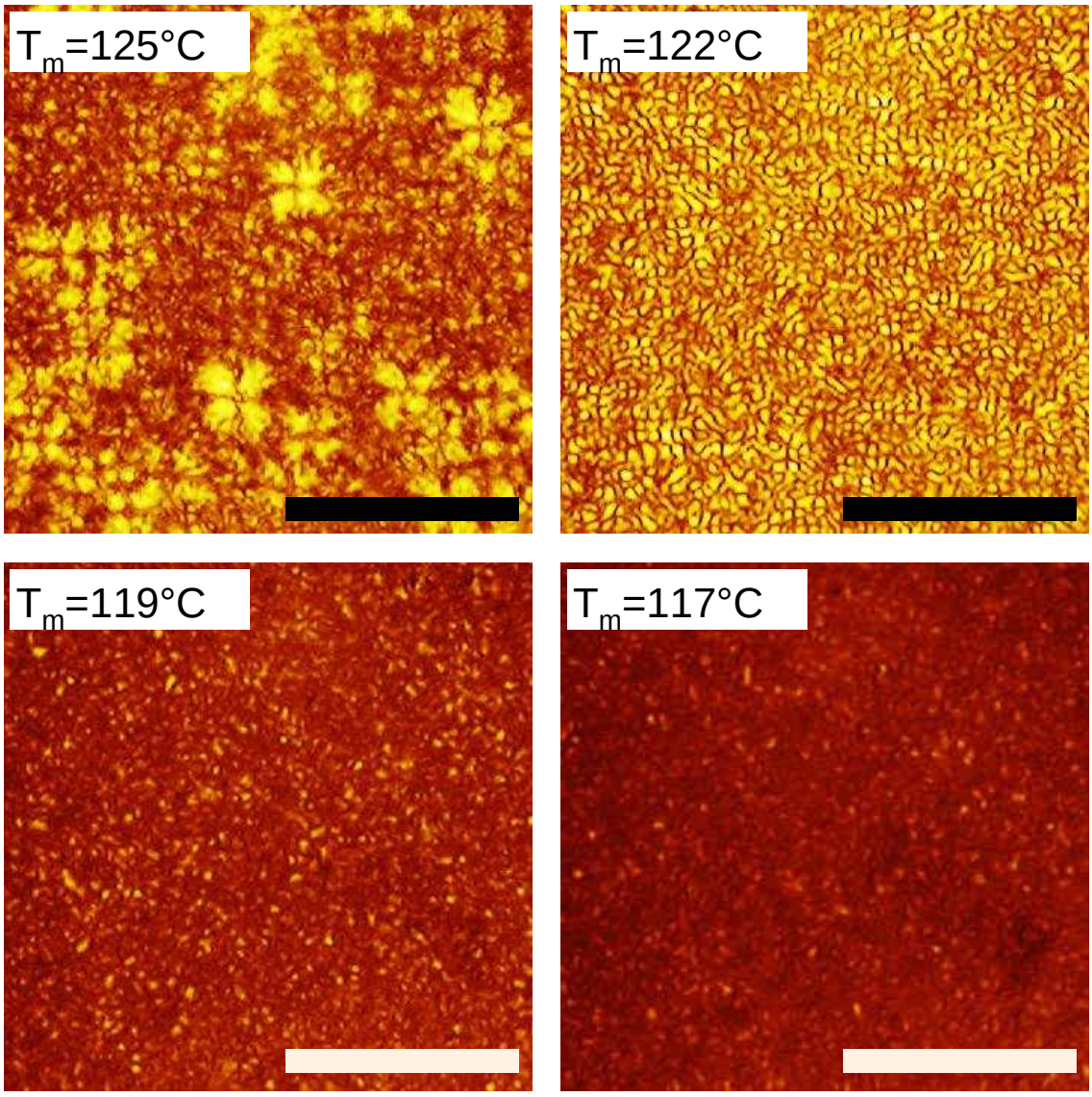

Figure 10: POM images of different final states reached after isothermal crystallizations at 93 °C. Samples were heated from ambient to various melt temperatures T_{m} and then rapidly cooled to the crystallization temperature. The sticks have a length of 100μm

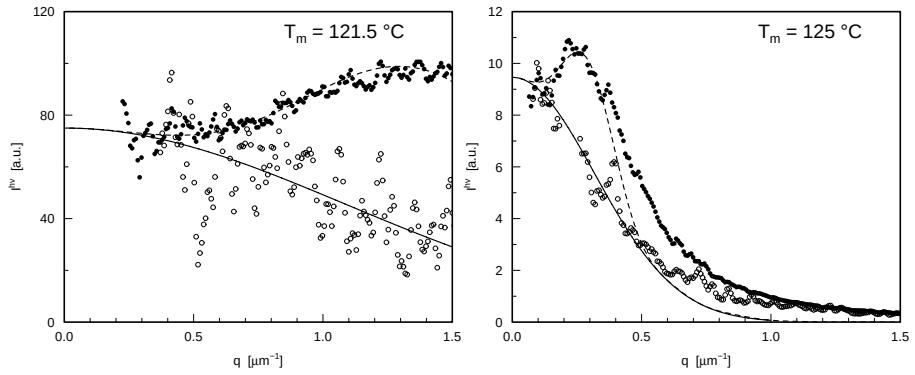

Figure 11: PEcO14: hv-light scattering patterns registered after an isothermal crystallization at 93 °C for two different melt temperatures T_{m} prior to cooling. Intensity distribution along the equator (*open symbols*) and variation of the azimuthal average in radial direction (*filled symbols*)

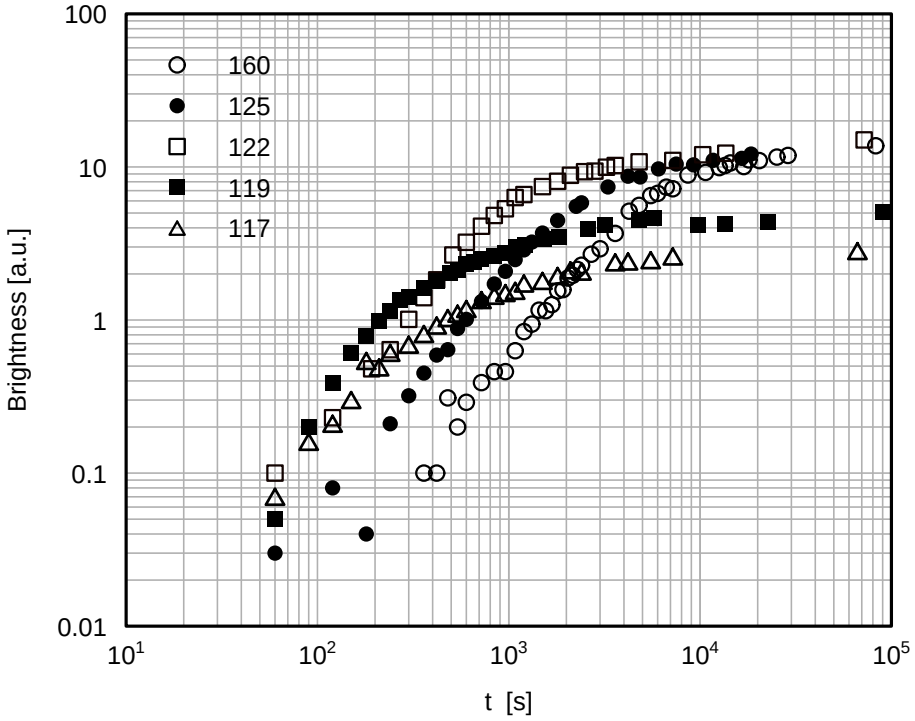

Figure 12: Isothermal crystallization at 93 °C for different melt temperatures prior to cooling (117 °C to 160 °C): Time dependence of the image brightness

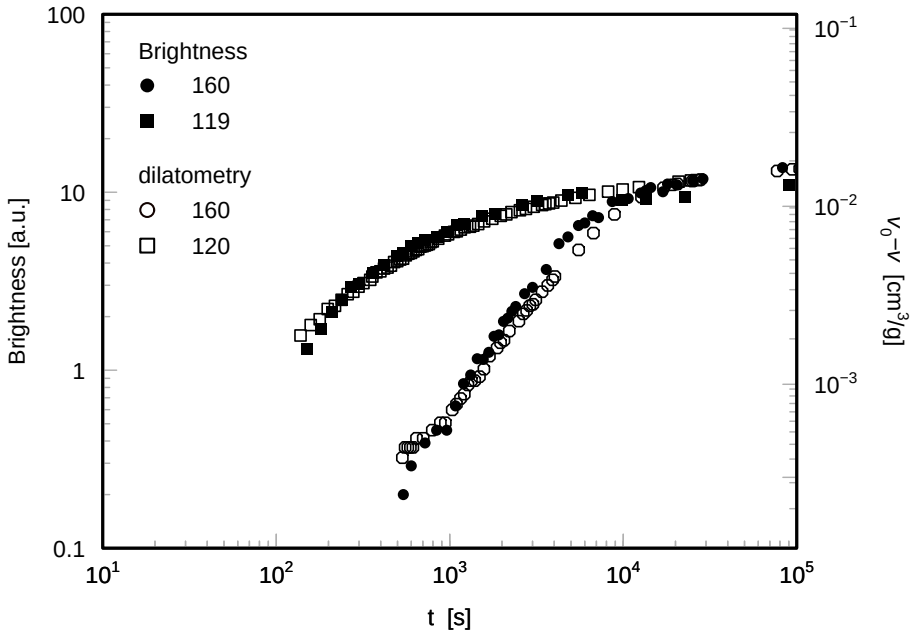

Figure 13: Isothermal crystallization at 93 °C for two different melt temperatures prior to cooling (119/120 °C and 160 °C): Time dependence of the image brightness compared to the change of the specific volume

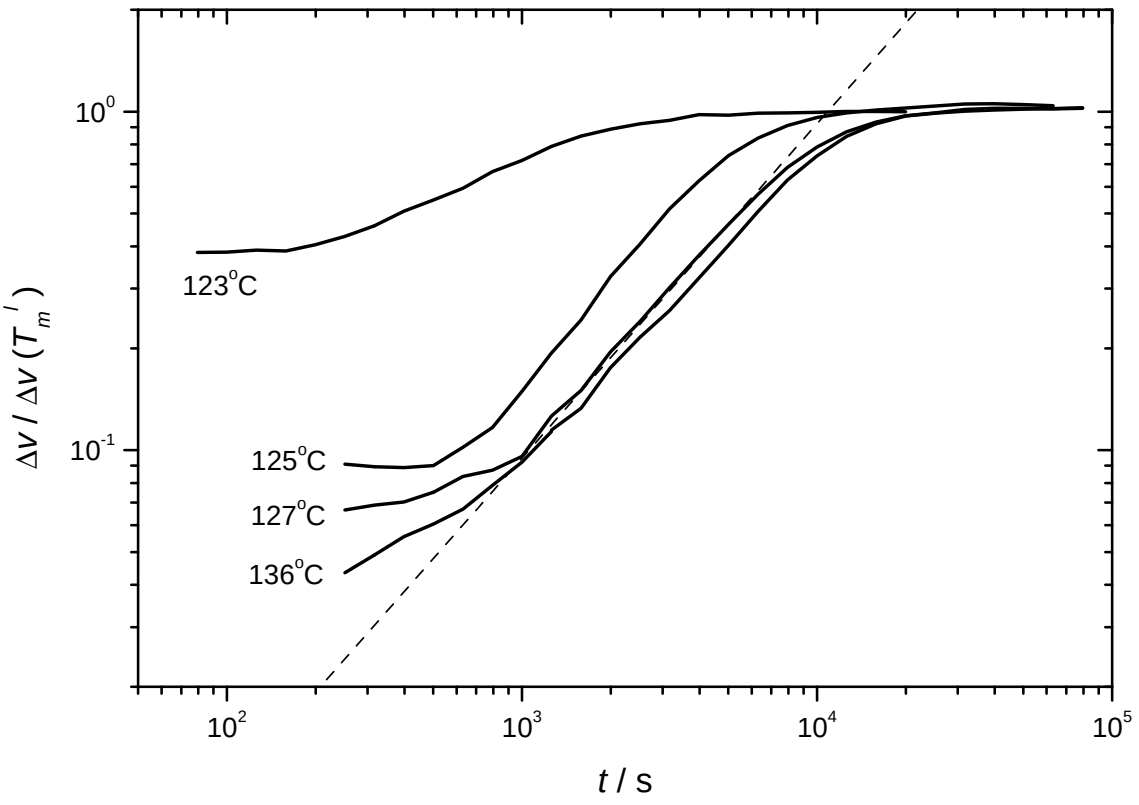

Figure 14: Derived from the data in Fig.5: Time dependence of the ratio between the isothermal volume change Δv observed for melt temperatures $T_{\rm m}$=125 °C, 127 °C and 136 °C and the isothermal volume change $\Delta v(T_{\rm m}^{\rm l})$ in the low melt temperature limit

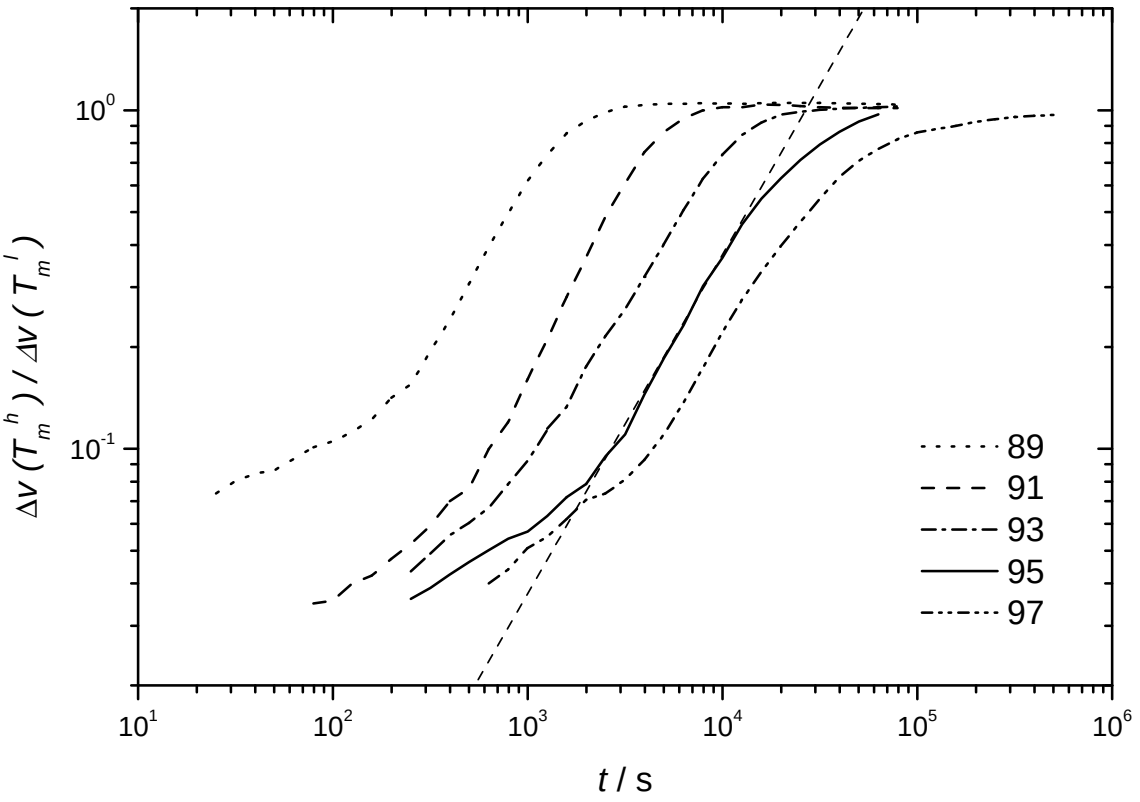

Figure 15: Derived from the data in Fig.6: Time dependent ratios between the values on the isotherms associated with the high and the low melt temperature limit

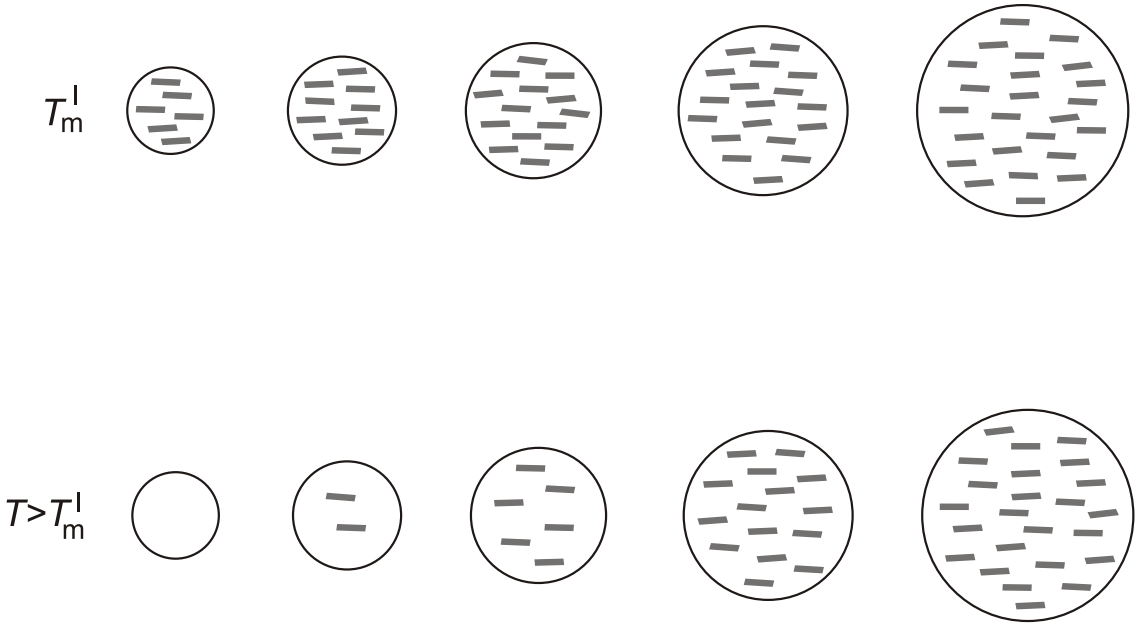

Figure 16: Schematic describing the melt memory effect on the first order crystallization mode. The spheres are representatives of the volume occupied by objects of the precursor structure. It grows in size and is simultaneously filled with crystallites. The upper row refers to the process in the low T_m limit where the objects are always completely filled, the lower row describes the development at a higher T_m where the crystal nucleation is delayed